Septal annular dilation in chronic ovine functional tricuspid regurgitation

Artur Iwasieczko, MD,[a,b] Tomasz Jazwiec, MD,[c] Manikantam Gaddam, PhD,[a] Boguslaw Gaweda, MD,[a,b] Magdalena Piekarska, MD,[a] M. Solarewicz, BS,[a] Manuel K. Rausch, PhD,[d] and Tomasz A. Timek, MD, PhD[a]

ABSTRACT

Introduction: Annular reduction with prosthetic rings represents the current surgical treatment of functional tricuspid regurgitation (FTR). However, alterations of annular geometry and dynamics associated with FTR are not well characterized.

Methods: FTR was induced in 29 adult sheep with either 8 weeks of pulmonary artery banding (PAB, n = 15) or 3 weeks of tachycardia-induced cardiomyopathy (TIC, n = 14). Eight healthy sheep served as controls (CTL). At the terminal procedure, all animals underwent sternotomy, epicardial echocardiography, and implantation of sonomicrometry crystals on the tricuspid annulus (TA) and right ventricular free wall while on cardiopulmonary bypass. Simultaneous hemodynamic, sonomicrometry, and echocardiographic data were acquired after weaning from cardiopulmonary bypass and stabilization. Annular geometry and dynamics were calculated from 3-dimensional crystal coordinates.

Results: Mean FTR grade (0-4) was 3.2 ± 1.2 and 3.2 ± 0.5 for PAB and TIC, respectively, with both models of FTR associated with similar degree of right ventricular dysfunction (right ventricular fractional area contraction 38 ± 7% and 37 ± 9% for PAB and TIC, respectively). Left ventricular ejection fraction was significantly reduced in TIC versus baseline (33 ± 9%, vs 58 ± 4%, $P = .0001$). TA area was 651 ± 109 mm², 881 ± 242 mm², and 995 ± 232 mm² for CTL, FTR, and TIC, respectively ($P = .006$) with TA area contraction of 16.6 ± 4.2%, 11.5 ± 8.0%, and 6.0 ± 4.0%, respectively ($P = .003$). Septal annulus increased from 33.8 ± 3.1 mm to 39.7 ± 6.4 mm and 43.1 ± 3.2 mm for CTL, PAB, and TIC, respectively ($P < .0001$).

Conclusions: Ovine FTR was associated with annular dilation and reduced annular area contraction. Significant dilation of septal annulus was observed in both models of FTR. As tricuspid rings do not completely stabilize the septal annulus, continued remodeling may contribute to recurrent FTR after repair. (J Thorac Cardiovasc Surg 2023;■:1-10)

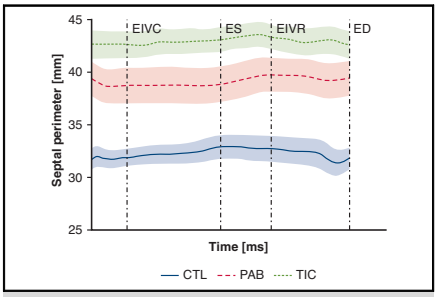

Septal annulus throughout the cardiac cycle in CTL, PAB, and TIC animals.

CENTRAL MESSAGE

Chronic ovine FTR with and without left ventricular dysfunction was associated with significant tricuspid annular dilation and lengthening of the septal portion of the annulus.

PERSPECTIVE

Currently used annuloplasty bands used to treat FTR leave variable portions of the septal annulus unsupported. Our data suggest that the septal annulus dilates significantly in severe FTR and may contribute to high recurrence rates. These data may better guide design of annuloplasty prostheses.

See Commentary on page XXX.

Functional tricuspid regurgitation (FTR) is clinically associated with tricuspid annular dilation and right ventricular dysfunction and remodeling, yet the pathophysiology of valve insufficiency is incompletely understood.[1] Repair with prosthetic ring annuloplasty represents the contemporary approach to FTR to reduce and stabilize the anterior and posterior portions of the tricuspid annulus (TA) that are believed to dilate during evolution of FTR.[2] This strategy, however, is associated with high rates of residual and recurrent insufficiency in the setting of severe

From the [a]Division of Cardiothoracic Surgery, Corewell Health, Grand Rapids, Mich; [b]Clinical Department of Cardiac Surgery, St Jadwiga Provincial Clinical Hospital, Rzeszow, Poland; [c]Department of Cardiac Surgery, School of Medicine in Katowice, Medical University of Silesia, Katowice, Poland; and [d]Departments of Aerospace Engineering & Engineering Mechanics, Biomedical Engineering, University of Texas at Austin, Austin, Tex.

The study was funded by internal grant from the Meijer Heart and Vascular Institute at Corewell Health and National Institute of Health R01HL165251 (M.K.R. and T.A.T.) and R21HL161832 (M.K.R. and T.A.T.). A.I. and T.J. were Peter C. and Pat Cook Endowed Research Fellows in Cardiothoracic Surgery.

Received for publication Jan 29, 2023; revisions received March 19, 2023; accepted for publication April 5, 2023.

Address for reprints: Tomasz A. Timek, MD, PhD, Section of Cardiac Surgery, Corewell Health, Michigan State University College of Human Medicine, 100 Michigan Ave SE, Grand Rapids, MI 49503 (E-mail: Tomasz.Timek@corewellhealth.org).

0022-5223/$36.00

https://doi.org/10.1016/j.jtcvs.2023.04.003

Abbreviations and Acronyms
CTL = control
ECG = electrocardiography
FTR = functional tricuspid regurgitation
IV = intravenous
LV = left ventricular
PAB = pulmonary artery banding
RV = right ventricle
TA = tricuspid annulus
TIC = tachycardia-induced cardiomyopathy

Scanning this QR code will take you to the table of contents to access supplementary information.

FTR.[3,4] Some investigators have suggested isolated ring annuloplasty is insufficient to treat severe FTR, as associated ventricular and subvalvular geometric perturbations are already advanced,[1] but the detailed 3-dimensional geometry of the TA in severe FTR has not been well described. A recent clinical study demonstrated that all segments of the TA, including the septal annulus, enlarge during progression of FTR.[5] Therefore, currently available annular prostheses[6] may not adequately support the dilated annulus, as all leave a portion of the septal annulus unsupported. It is feasible that continued dilation of this segment of the annulus in severe FTR may contribute to residual and recurrent insufficiency after repair. As such, more detailed knowledge of tricuspid annular dynamics and geometry in the setting of severe FTR may lead to more rational prosthesis design and improved reparative techniques. With this goal in mind, we set out to investigate tricuspid annular geometry and dynamics in 2 chronic ovine models of right ventricular dysfunction and clinically significant FTR.

METHODS

All animals received humane care in compliance with the Principles of Laboratory Animal Care. The study protocols were approved by Calvin University Institutional Animal Care and Use Committee protocol number 2018-438 and Michigan State University Institutional Animal Care and Use Committee protocol number 2020-35 approved on July 27, 2020.

Surgical Preparation

A total of 47 adult healthy Dorset male sheep (age 9-12 months) were used for the study. We chose to use the ovine model, as sheep are sturdy experimental animals that tolerate cardiac procedures well and are docile and easy to take care of postoperatively. Their body size and hearts are of human size, facilitating clinical procedures and imaging. FTR was induced in 2 groups of animals either through pulmonary artery banding (PAB, n = 20) or tachycardia-induced cardiomyopathy (TIC, n = 19), and remaining sheep served as controls (CTL, n = 8). Experimental animals underwent the respective procedure to induce FTR and subsequent terminal surgery whereas control animals underwent terminal surgery only.

Tachycardia-Induced Cardiomyopathy (TIC)

The surgical protocol for TIC has been described in detail previously[7] and will be presented here in abbreviated form. An external right jugular intravenous (IV) catheter was placed under local anesthesia with 1% lidocaine and subsequently animals were anesthetized with propofol (2-5 mg/kg IV), intubated, and mechanically ventilated. General anesthesia was maintained with inhalational isoflurane (1%-2.5%) and fentanyl (5-20 mg/kg/min). A sterile left minithoracotomy through the sixth intercoastal space was used to suture a monopolar pacing lead onto the lateral left ventricular (LV), wall which was exteriorized to a pacemaker (Consulta CRT-P; Medtronic) placed in the subcutaneous pocket near the spine. Control epicardial echocardiography was performed to assess biventricular function and valvular competence. The surgical incision was then approximated in standard fashion, and intercostal nerves in the region were infiltrated with 0.25% bupivacaine. After a 5-day recovery period, high-rate pacing protocol was initiated as described previously.[8] Animals were paced for a mean of 22 ± 6 days at a rate of 200 to 240 bpm until LV dysfunction (LV ejection fraction <30%) was seen on surveillance transthoracic echocardiography. Furosemide was used to treat symptoms of heart failure based on clinical examination. Subsequently, the pacer was turned off for 24 hours, and the animals were returned to the operating room for the terminal study.

Pulmonary Artery Banding (PAB)

The same anesthetic protocol as described previously was used for the PAB procedure. A limited sterile left thoracotomy was made through the fourth intercoastal space, and epicardial echocardiography was performed to assess biventricular function and valvular competence. The internal mammary artery and main pulmonary artery were cannulated for simultaneous systemic and pulmonary pressure monitoring. An umbilical tape was used to encircle the main pulmonary artery and progressively tightened down with successive clip approximations until development of systemic blood pressure instability, at which time the last clip was removed.[9] Proximal pulmonary artery pressure after the removal of last clip was then recorded. The thoracotomy was subsequently closed, and the animals were extubated and monitored for 8 weeks with intermittent treatment with furosemide for evolving heart failure symptoms. Thoracentesis was performed occasionally when significant pleural fluid was diagnosed on surveillance echocardiography. After 8 weeks, the animals were returned to the operating room for the terminal procedure.

Terminal Procedure

All experimental and control animals underwent the terminal procedure for sonomicrometry crystal implantation. After induction of anesthesia as described previously, a 4-Fr vascular access sheath was introduced through left carotid artery for arterial blood pressure measurements. Animals were fully heparinized, and the right carotid artery and right internal jugular vein were exposed in preparation for cardiopulmonary bypass. The operative procedure was performed through a sternotomy and the heart was exposed in a pericardial cradle. Epicardial echocardiography was repeated to assess biventricular function and valvular competence (Videos 1 and 2). A multistage 21-F venous cannula was placed via the right jugular vein and advanced to the inferior vena cava, and arterial access was achieved using a 17-F carotid artery cannula. While on cardiopulmonary bypass and with the heart beating, both cava were snared and the right atrium opened. Six (2-mm) sonomicrometry crystals (Sonometrics Corporation) were implanted around the TA with one crystal at each commissure and one equidistant between the commissures (Figure 1). Thirteen crystals were implanted on the right ventricular epicardium along 3 equators of the right

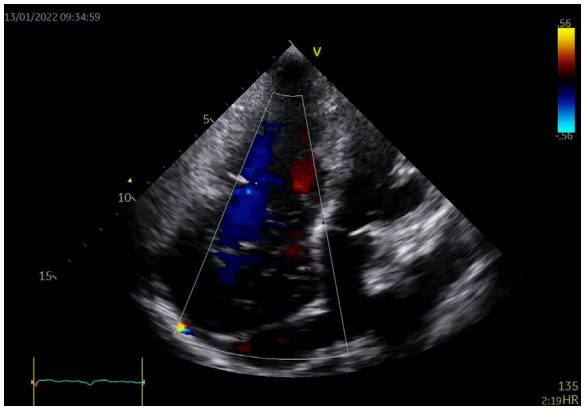

VIDEO 1. Video images of epicardial echocardiography at the time of the terminal study in a PAB animal. Video available at: https://www.jtcvs.org/article/S0022-5223(23)00324-0/fulltext.

ventricular free wall with additional crystal at the right ventricular apex. Pressure transducers (PA4.5-X6; Konigsberg Instruments, Inc) were placed in the right and left ventricle through the apex and in the right atrium. An electrocardiography (ECG) electrode connected to the sonomicrometry system was sutured to the right ventricular free wall. The animal was weaned from cardiopulmonary bypass and allowed to stabilize for 30 minutes to achieve steady state hemodynamics. Every animal received lidocaine IV drip (0.03 mg/kg/min) to prevent ventricular ectopy. All animals were studied under open-chest experimental conditions and simultaneous hemodynamic, and sonomicrometry data were acquired. At the conclusion of the experiment, the animals were killed by administering sodium pentothal (100 mg/kg IV). The heart was excised, and proper placement of annular and ventricular crystals was confirmed.

Data Acquisition

Epicardial echocardiography to evaluate biventricular function and valvular insufficiency was performed with a 1.5- to 3.6-MHz transducer and Vivid S6 ultrasound machine (GE Healthcare). The degree of valvular insufficiency was assessed using American Society of Echocardiography criteria. The grading included comprehensive evaluation of color flow and continuous-wave Doppler. TR was graded accordingly and categorized

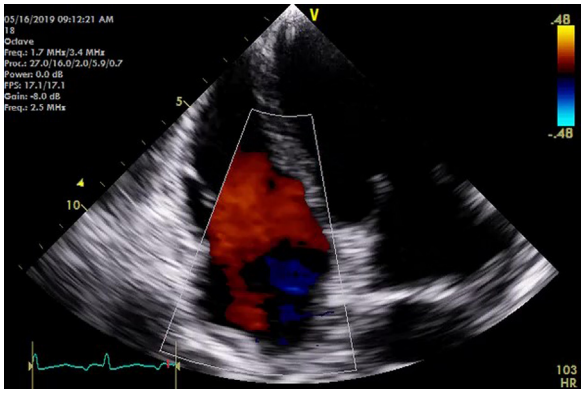

VIDEO 2. Video images of epicardial echocardiography at the time of the terminal study in a TIC animal. Video available at: https://www.jtcvs.org/article/S0022-5223(23)00324-0/fulltext.

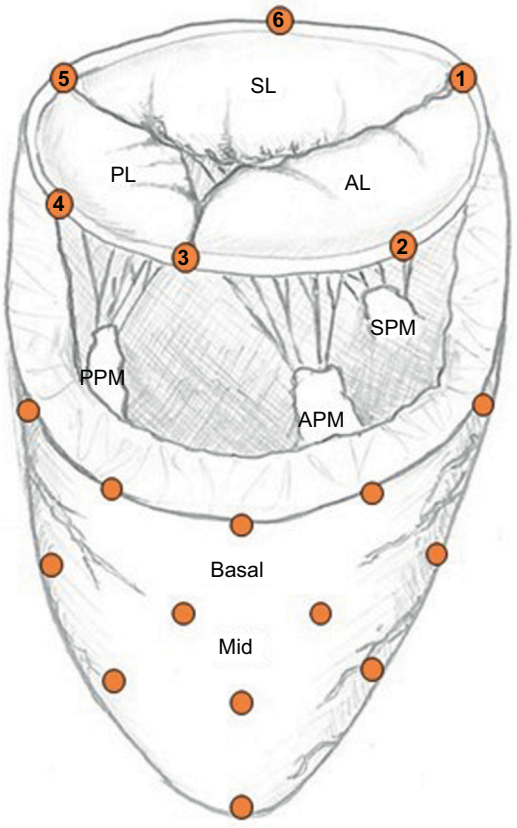

FIGURE 1. Schematic representation of the right ventricle with implanted sonomicrometry crystals (*orange spheres*) around the tricuspid annulus and on the right ventricular epicardium. Crystals #1-2-3 correspond to the anterior annulus, #3-4-5 to the posterior annulus, and #5-6-1 to the septal annulus. *SL*, Septal leaflet; *PL*, posterior leaflet; *AL*, anterior leaflet; *SPM*, septal papillary muscle; *PPM*, posterior papillary muscle; *APM*, anterior papillary muscle.

by an experienced echo sonographer (J.B.) as none or trace (0), mild (+1), moderate (+2), or moderately severe (+3), or severe (+4).

All sonomicrometry data were acquired using a Sonometrics Digital Ultrasonic Measurement System DS3 (Sonometrics Corporation) as previously described.[10] Data were acquired at 128 Hz with simultaneous left ventricular pressure, right ventricular pressure, central venous pressure, and ECG recordings. Data from 3 consecutive cardiac cycles during normal sinus rhythm were averaged for each animal. All sonomicrometry recordings were analyzed with custom MATLAB code. End-diastole was defined as the time of the beginning of positive deflection in ECG voltage (R wave) whereas end-systole was determined as the time of maximum negative dp/dt of left ventricular pressure.

Data Analysis

Right ventricle (RV) volume was calculated using convex hull method based on epicardial and annular crystal coordinates. Annular centroid of all annular crystals was calculated and was subsequently used for transformation and rotation of point clouds with centroid as an origin and normal vector along with +z direction. A spline curve was fit along those 6 points to replicate the annulus. Triangular areas formed by those sequenced points and the centroid were all added to calculate tricuspid annular area. Similarly, perimeter was measured using the distance between the adjacent points along the spline. Tricuspid annular anterior–posterior diameter

TABLE 1. Hemodynamic and echocardiographic parameters before and after induction of FTR in PAB and TIC animals

	Pre-PAB	PAB	Pre-TIC	TIC
TR (+0-4)	0.4 ± 0.5	3.2 ± 1.2*	0 ± 0	3.1 ± 0.9*
MR (+0-4)	0 ± 0	1.1 ± 0.5*	0 ± 0	2.2 ± 0.8*
RVFAC, %	54 ± 4	38 ± 7*	54 ± 7	37 ± 9*
TAPSE	1.2 ± 0.1	0.8 ± 0.1*	1.3 ± 0.2	1.1 ± 0.3
TAD, mm	2.4 ± 0.2	3.1 ± 0.2*	2.5 ± 0.3	3.2 ± 0.5*
LVEF, %	63 ± 3	58 ± 4*	62 ± 8	33 ± 8*

Values are mean ± standard deviation. *PAB*, Pulmonary artery banding; *TIC*, tachycardia-induced cardiomyopathy; *TR*, tricuspid regurgitation; *MR*, mitral regurgitation; *RVFAC*, right ventricular fractional area contraction; *TAPSE*, tricuspid annulus plane systolic excursion; *TAD*, tricuspid annulus diameter; *LVEF*, left ventricular ejection fraction. *$P < .05$ versus pre- by Student *t* test for dependent observations.

was calculated as the distance between annular crystals #1 and # 4 and septal–lateral diameters as distance between crystal #6 and #2 (Figure 1). In addition, an ellipse was fit through the annular crystals using MATLAB program to obtain eccentricity (e), which defines the circularity of annulus (e = 0 for a perfectly circular annulus while e > 0 for an ellipse). Green–Lagrange Strains were calculated for TA throughout the cardiac cycle with strain at maximal diastolic annular size as the reference configuration. In-house MATLAB calculations were performed to project mean values on to average annular configuration (spatial data) and VTK files were generated. These files were later imported to ParaView 5.0.0 (Kitware Inc, Open-source software, Sandia National Laboratories, Los Alamos National Laboratories) for temporal (end-isovolumetric contraction, end-isovolumetric relaxation, end-systole) visualization of strains for CTL, PAB, and TIC annulus.

All the data are presented as a mean with standard deviation, and measured parameters were compared between CTL, PAB, and TIC using analysis of variance with Bonferroni correction.

RESULTS

With PAB, mean pulmonary artery pressure in the animals receiving PAB increased from 15 ± 2 mm Hg to 36 ± 5 mm Hg ($P = .0001$). Three animals who received PAB died during the banding procedure, one each from stroke, pulmonary artery hemorrhage, and acute right heart failure. Seventeen surviving animals had echocardiographic assessment after 8 weeks of follow-up, which revealed that 11 animals developed severe TR, 4 developed moderate insufficiency, and 2 did not develop significant TR and were excluded for final study number of 15 PAB animals. In the TIC group, 3 animals died during the pacing protocol, and follow-up echocardiography in remaining 16 demonstrated severe TR in 6 animals, moderate-severe in 4, moderate in 5, and 1 animal without significant TR which was excluded. One TIC animal was excluded because of poor sonomicrometry data quality yielding final study number of 14 TIC animals. Hemodynamic and echocardiographic parameters before and after induction of FTR in PAB and TIC animals are demonstrated in Table 1. Both models of FTR were associated with similar degree of RV dysfunction, annular dilatation, and level of tricuspid insufficiency. As may be expected, TIC resulted in significant concurrent LV dysfunction and functional mitral regurgitation that was not observed in PAB. Hemodynamic parameters of all animal groups at the time of data collection during the terminal study are summarized in Table 2. Experimental animals had greater heart rates, but systolic blood pressure was not different between CTL, PAB, and TIC. PAB was associated with greater peak RV systolic pressure, whereas greater central venous pressure was seen with TIC. Right ventricular end-diastolic volume calculated based on annular and free wall crystals was 126 ± 13, 176 ± 32, and 135 ± 26 mL for CTL, PAB, and TIC, respectively. ($P < .001$). Sonomicrometry-derived measurements of annular dynamics and geometry are shown in Table 3. Significant annular area and diameter increase versus CTL was seen in both PAB and TIC, whereas the greatest reduction in annular area and perimeter contraction during the cardiac cycle was observed with TIC. Annular area at end-systole increased approximately 36% in PAB and 52% in TIC relative to control animals. Regionally, the posterior annulus enlarged little at end-systole with PAB and TIC whereas the anterior annulus increased by 13% and 24% with

TABLE 2. Hemodynamic parameters of all animal groups at the time of data collection during the terminal study

	CTL (n = 8)	PAB (n = 15)	TIC (n = 14)	ANOVA (*P*)
Weight, kg	63 ± 4	63 ± 3	57 ± 5*	<.001
HR, bpm	88 ± 11	108 ± 16*	126 ± 13*	<.001
LVP, mm Hg	98 ± 11	88 ± 18	91 ± 16	.355
RVP, mm Hg	30 ± 7	45 ± 15*	39 ± 10	.015
CVP, mm Hg	12 ± 1	12 ± 2	19 ± 5*	<.001

Values are mean ± standard deviation. *CTL*, Control; *PAB*, pulmonary artery banding; *TIC*, tachycardia-induced cardiomyopathy; *ANOVA*, analysis of variance; *HR*, heart rate; *LVP*, left ventricular pressure; *RVP*, right ventricular pressure; *CVP*, central venous pressure. *$P < .05$ vs CTL with Bonferroni correction.

TABLE 3. Sonomicrometry-derived measurements of annular dynamics and geometry

	CTL (n = 8)	PAB (n = 15)	TIC (n = 14)	ANOVA (*P*)
TAA, mm^2	651 ± 109	886 ± 242*	995 ± 232*	.006
TAA contraction, %	16.6 ± 4.2	11.5 ± 8.0	6 ± 4*	.003
CC distance, mm				
AS-PS (1-5)	28.8 ± 2.8	32.2 ± 5.0	35.3 ± 2.6*	.003
AS-AP (1-3)	20.3 ± 4.6	25.9 ± 5.5*	28.1 ± 4.5*	.007
AP-PS (3-5)	30.0 ± 5.1	31.7 ± 4.7	30.5 ± 4.7	.699
TA diameter, mm				
AP	26.6 ± 2.7	32.0 ± 5.7*	34.7 ± 3.9*	.010
SL	24.3 ± 3.3	29.4 ± 5.0*	31.7 ± 3.4*	.018
TAP, mm	95.8 ± 8.1	107.7 ± 15.3	114.5 ± 9.5*	.007
TAP contraction, %	7.4 ± 1.7	5.5 ± 3.8	3.5 ± 2.7*	.027
Regional TAP, mm				
Anterior (1-2-3)	28.7 ± 4.9	32.6 ± 7.4	35.6 ± 5.6	.075
Posterior (3-4-5)	36.3 ± 6.4	38.1 ± 6.0	36.1 ± 4.4	.615
Septal (5-6-1)	33.7 ± 3.1	39.7 ± 6.4*	43.1 ± 3.2*	.001
Regional TAP contraction, %				
Anterior (1-2-3)	11.6 ± 2.8	6.9 ± 5.1	6.1 ± 5.7*	.057
Posterior (3-4-5)	10.5 ± 3.8	7.4 ± 5.3	8.5 ± 7.4	.536
Septal (5-6-1)	5.9 ± 1.8	5.4 ± 3.1	5.4 ± 3.8	.933

Values are mean ± standard deviation. *CTL*, Control; *PAB*, pulmonary artery banding; *TIC*, tachycardia-induced cardiomyopathy; *ANOVA*, analysis of variance; *TAA*, tricuspid annular area; *Contraction*, % reduction during cardiac cycle; *CC*, commissure–commissure; *AS*, anteroseptal; *PS*, posterior-septal; *AP*, anteroposterior; *TA*, tricuspid annulus, *SL*, septal-lateral; *TAP*, tricuspid annular perimeter. *$P < .05$ vs CTL by Student *t* test for independent comparisons with Bonferroni correction.

PAB and TIC, respectively. Surprisingly, the septal segment was 17% longer in PAB and 28% longer in TIC. As the TIC animals had significantly lower body weights, septal segment length-to-weight ratio was used for a more direct comparison. Septal segment length-to-weight ratio was 0.5 ± 0.1, 0.6 ± 0.1, and 0.8 ± 0.1 mm/kg for CTL, PAB, and TIC, respectively ($P < .001$ by analysis of variance). In this analysis, the septal segment was significantly longer in TIC versus PAB animals ($P < .05$). Overall, the septal annulus underwent greatest dilation in both PAB and TIC whereas the anterior annulus had the greatest reduction in contractile function. Annular area and perimeter throughout the cardiac cycle are shown in Figure 2 with annular diameters and eccentricity summarized in Figure E1. Anterior, posterior, and septal annular segment lengths during the cardiac cycle are depicted in Figure 3. Two-dimensional reconstructions of the TA with regional strain maps relative to maximal diastolic annular area in CTL, PAB, and TIC are shown in Figure 4. Negative annular strain (contraction) was observed already at end-diastole, indicative of presystolic annular contraction. Anterior portion of the annulus appeared the most dynamic with reduced strain with PAB and TIC. These reconstructions also illustrate the enlargement and circularization of the annulus. Three-dimensional shape of the TA was determined as the deviation of each annular crystal from the annular plane determined by the 3D coordinates of all annular crystals. These data for all studied animals are schematically summarized in Figure E2, which revealed that the 3-dimensional shape of the TA did not change significantly with functional TR.

DISCUSSION

Dilation of the TA is central to the pathophysiology of FTR, yet the detailed 3-dimensional geometry and dynamics of the TA associated with FTR have not been fully characterized. Our experimental study using 2 different ovine models of FTR revealed significant annular area increase, reduced dynamic motion, and pronounced enlargement of the septal portion of the annulus.

The ovine model of pulmonary banding used in the study resulted in isolated RV dysfunction and moderately severe FTR, which is consistent with previous studies.[9] Rapid ventricular pacing, in contrast, was used to induce an ovine model of FTR in the setting of biventricular failure.[7] Echocardiographic findings in both models demonstrated reduced RV function, chamber enlargement, and annular dilatation, all consistent with experimental observations of other investigators[11] and clinical reports in patients with functional TR.[12] Recent 3-dimensional echocardiographic assessment of normal human TV annulus revealed 35 ± 10% area reduction during the cardiac cycle with maximal size observed in late diastole before atrial contraction.[13] We also found maximal TA area in late diastole with significant presystolic contraction present as observed clinically. However, our TA area reduction of 16% in control

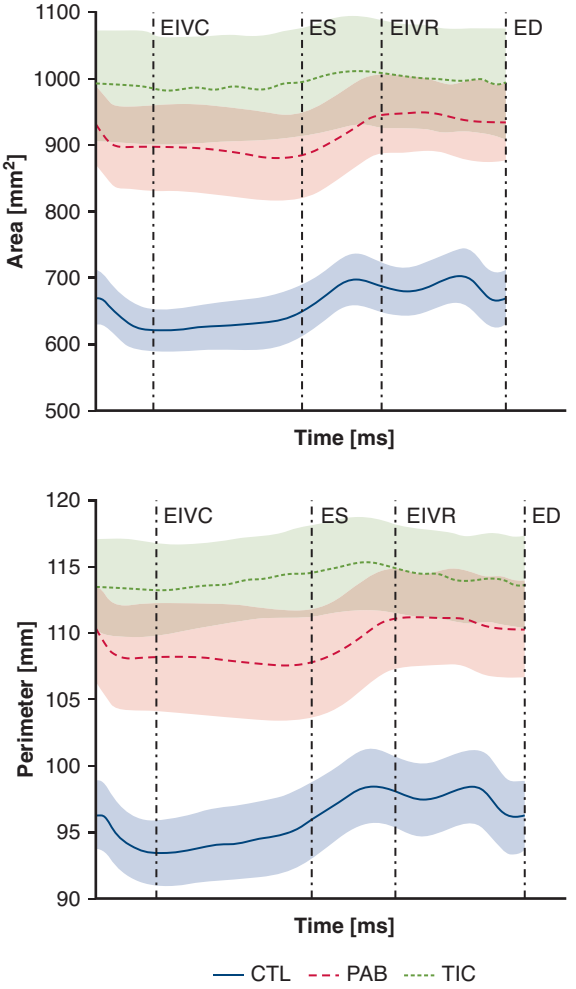

FIGURE 2. Group mean and standard deviation data for tricuspid annular area (*top panel*) and tricuspid annular perimeter (*bottom panel*) throughout the cardiac cycle in control (CTL = 8 [*black line*]), pulmonary artery banding (PAB = 15 [*dashed blue line*]), and tachycardia-induced cardiomyopathy (TIC = 14 [*dashed orange line*]) animals. *EIVC*, End-isovolumic contraction; *ES*, end-systole; *EIVR*, end-isovolumic contraction; *ED*, end-diastole; *CTL*, control; *PAB*, pulmonary artery banding; *TIC*, tachycardia-induced cardiomyopathy.

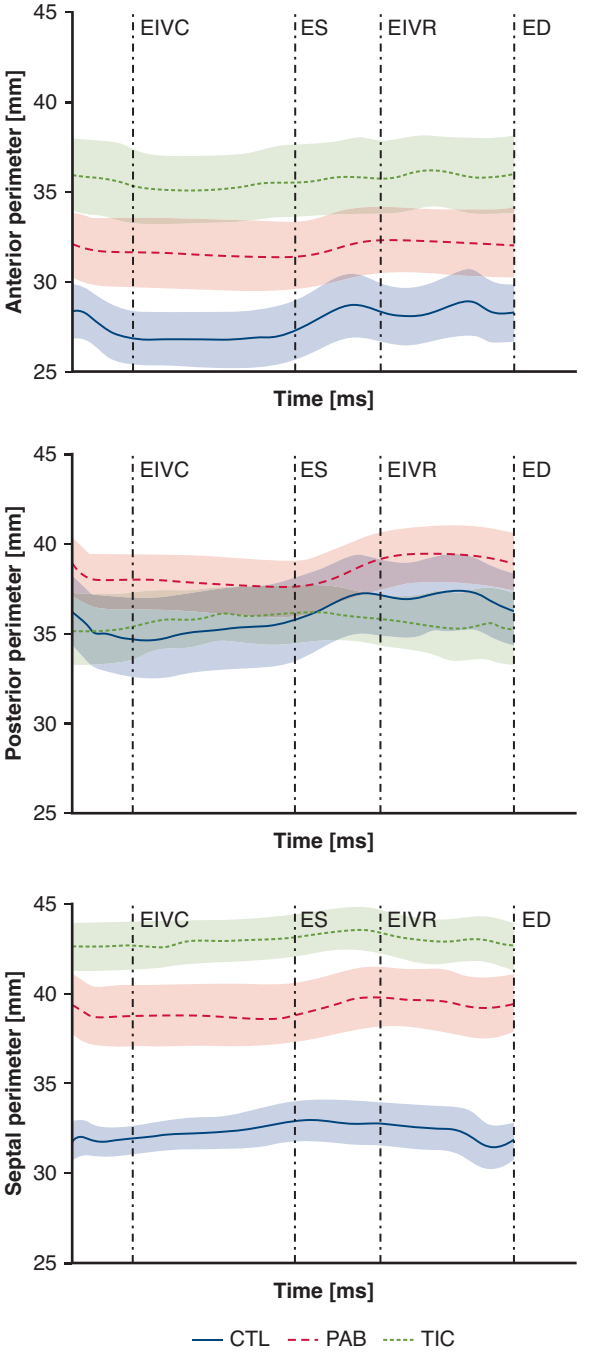

FIGURE 3. Group mean and standard deviation data for anterior (*top panel*), posterior (*middle panel*), and septal (*bottom panel*) annular perimeter throughout the cardiac cycle in control (CTL = 8 [*black line*]), pulmonary artery banding (PAB = 15 [*dashed blue line*]), and tachycardia-induced cardiomyopathy (TIC = 14 [*dashed orange line*]) animals. *EIVC*, End-isovolumic contraction; *ES*, end-systole; *EIVR*, end-isovolumic contraction; *ED*, end-diastole; *CTL*, control; *PAB*, pulmonary artery banding; *TIC*, tachycardia-induced cardiomyopathy.

animals was not as remarkable but similar to that reported with sonomicrometry in pig (21%)[14] and sheep (22%)[15] experiments as well as ex vivo human hearts (11%).[16] Two- and three-dimensional echocardiographic studies of normal and dilated human hearts with at least moderate FTR have revealed that annular area increased by approximately 50% with greater circularization of annular shape.[17,18] These observations are consistent with our findings of approximately 36% to 52% annular increase at end-

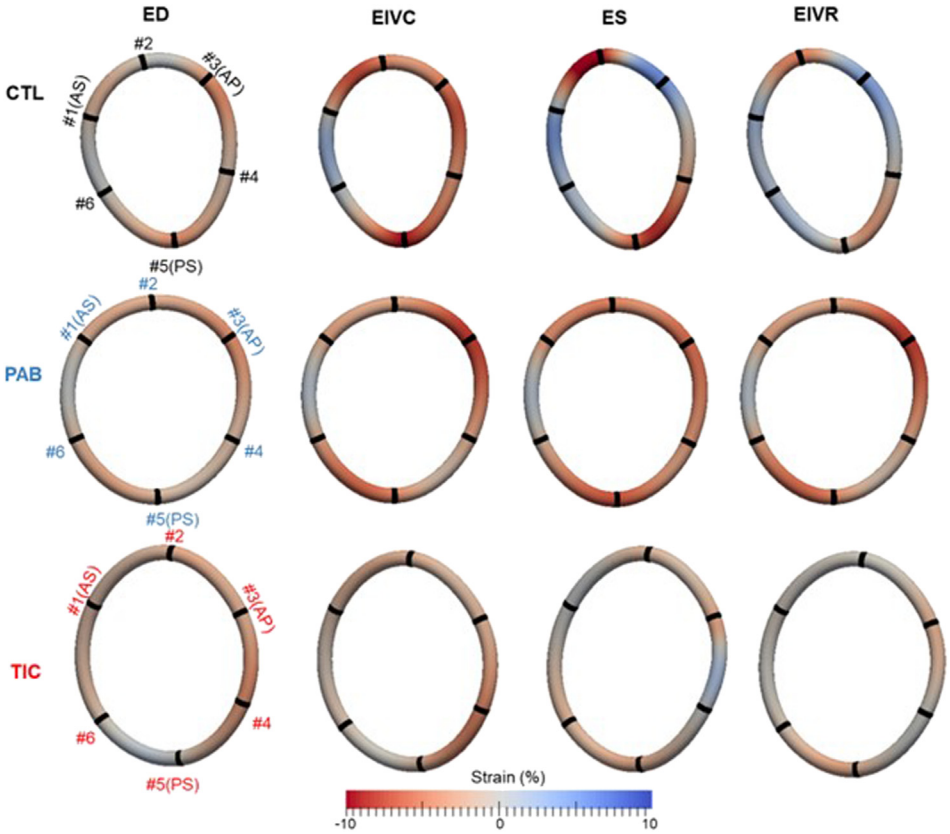

FIGURE 4. Tricuspid annular strain for control (CTL = 8 [*top panel*]), pulmonary artery banding (PAB = 15 [*middle panel*]), and tachycardia-induced cardiomyopathy (TIC = 14 [*bottom panel*]) animals at end-diastole (*ED*), end-isovolumic contraction (*EIVC*), end-systole (*ES*), and end-isovolumic relaxation (*EIVR*) versus maximal diastolic annular size. *Red color* indicates contraction, and *blue color* indicates elongation. *CTL*, Control; *AS*, anterior septal commissure; *AP*, anterior-posterior commissure; *PS*, posterior septal commissure; *PAB*, pulmonary artery banding; *TIC*, tachycardia-induced cardiomyopathy.

systole. In addition, annular area contraction was significantly reduced in patients with FTR[17] as demonstrated in our study. Both anterior-posterior and septal lateral annular diameters increased with FTR although more remarkably in TIC. These geometrical perturbations and changes in annular eccentricity are consistent with clinical findings in patients.[17,19]

The basis for annuloplasty reduction of the tricuspid anulus to treat FTR were derived from anatomical studies of Acar and colleagues,[2] who found that annular dilation in FTR occurred predominantly in the anterior and posterior portion of the annulus. However, these early pathologic studies included only 10 normal hearts and 15 hearts with rhematic heart disease and functional TR and may therefore not represent the full spectrum of anatomical variations. A recent pathologic study of the tricuspid valve in 100 hearts without valvular disease[20] revealed significant variation in annular anatomy. In particular, the posterior annulus length may range from 26% to 45% of total annular circumference depending on the number of posterior leaflet scallops, which may vary from 1 to 3. A smaller anatomical study of 27 normal hearts confirmed posterior leaflet scallop heterogeneity and established the posterior segment of the annulus as the largest annular segment.[21] However, the exact position of the anterior-posterior commissure remains difficult to standardize.[5,20,21] These data are consistent with our ovine findings with the posterior being the largest segment of the annulus in control animals. However, we were surprised to find that the septal annulus dilated remarkably in both our ovine models of RV failure and FTR. Interestingly, septal dilation was significantly greater in the setting of biventricular failure versus isolated right ventricular dysfunction, suggesting that left-sided myocardial compromise may further contribute to tricuspid annular dilation. Our previous acute ovine studies with mechanical unloading of the left ventricle[22] revealed reduction in tricuspid septal annular length suggesting an influence of left ventricular chamber size on the septal annulus and corroborating current data. A recent clinical study supports our experimental findings.[5] Direct intraoperative measurements of the TA in 317

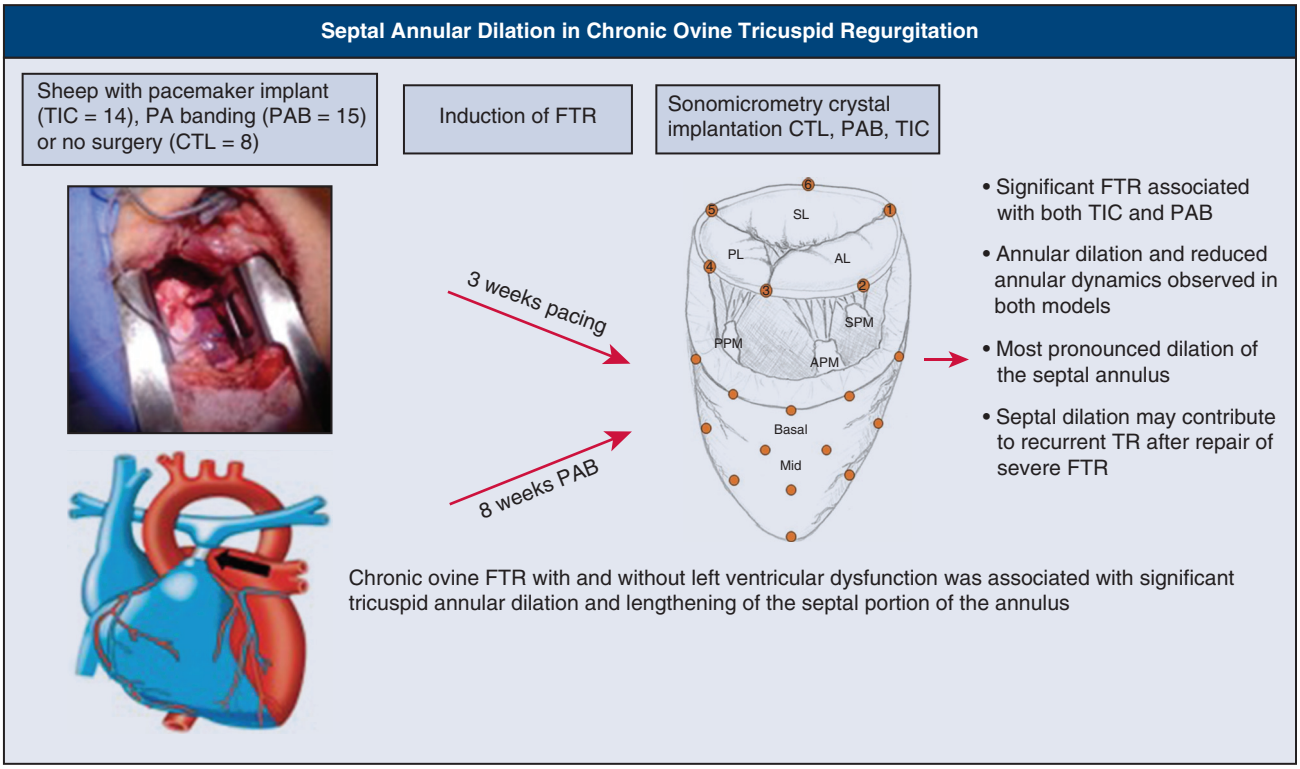

FIGURE 5. Graphic summary of experimental methods and key findings of the study. *TIC*, Tachycardia-induced cardiomyopathy; *PA*, pulmonary artery; *PAB*, pulmonary artery banding; *CTL*, control; *FTR*, functional tricuspid regurgitation; *PPM*, posterior papillary muscle; *SPM,* septal papillary muscle; *APM*, anterior papillary muscle; *PL*, posterior leaflet, *SL,* septal leaflet; *AL*, anterior leaflet.

patients with varying degrees of FTR reported that all segments of the TA dilate during progression from mild-to-severe FTR with 11.4% dilation in the septal annulus. It is feasible that this increase is substantially greater versus normal human hearts, as a healthy control group was not included in the study. Similarly, Kabasawa and colleagues[23] reported that on preoperative computed tomography imaging of patients undergoing TV repair the TA dilated in all segments proportionally. The septal annulus was found to be the longest of the 3 annular segments in patients with severe FTR in the study by Teng and collegues,[5] confirming our findings. Furthermore, dilation of the septal annulus was also reported to be the most sensitive predictor of postoperative recurrence of FTR, which may have implications for valvular repair. Although ring annuloplasty has been shown to be effective in patients with moderate or less FTR,[24] prosthetic annular reduction of severe FTR if fraught with high residual and recurrent TR rates.[3] Use of the rigid classic Carpentier-Edwards ring has been shown to offer better control of FTR progression in one study,[4] which may be related to its structure or more complete support of the annulus. In annuloplasty repair of severe FTR, Rodríguez-Palomares and colleagues[25] reported predischarge moderate or greater residual TR in 32.5% of patients, with 12.5% being severe. Most of the currently used tricuspid annular prostheses leave a variable portion of the septal annulus unsupported,[6] and progressive dilation may contribute to recurrent insufficiency. To this end, alterations of surgical technique have been introduced to better support the sepal annulus when performing prosthetic annular reduction in severe FTR.[26,27] Although these studies include only few patients, they have thus far yielded low recurrence rates at mid-term follow-up. Use of complete ring annuloplasty and septal plication was also demonstrated to be effective in correcting TR in a patient with massive annular dilation and FTR.[28] Based on the aforementioned data, the adequacy of open annuloplasty bands to treat severe FTR with annular dilation may need re-evaluation, and alternative surgical techniques or valve replacement warrant deliberation. Likewise, using the length of the septal annulus for sizing annuloplasty devices may also need reassessment. Surgically, septal plication and use of complete rings could be

considered to better stabilize the septal annulus and potentially improve control of FTR based on the current data; however, our study did not investigate any reparative techniques or their outcomes.

In conclusion, our experimental study using 2 ovine models of FTR revealed annular dilation and reduction of annular dynamics consistent with clinical findings in patients with significant FTR (Figure 5). We found that all segments of the TA dilated during evolution of FTR, but surprisingly most remarkably in the septal portion of the annulus, which was further exacerbated by left-sided dysfunction. These data may shed new light on the high failure rates of isolated annuloplasty repair of severe TR and guide more rational prosthesis design and novel reparative techniques to treat FTR.

Limitations

Our study has several important limitations that warrant caution in clinical extrapolation of these results. The data were collected in open-chest animals under general anesthesia, which can have a significant impact on RV function and TV dynamics, yet our previous studies in awake and anesthetized sheep did not show large effects on annular dynamics.[29] PAB was used to establish right ventricular pressure overload with associated RV dysfunction and FTR and as such does not reflect clinical disease. However, experimental afterload-based models may be more reliable to induce FTR, as clinical studies have shown that volume overload even when associated with RV dilation does not lead to significant valvular insufficiency.[30] Our model of FTR associated with TIC presents a rare form of clinical TR and was induced over a 3-week period again not reflecting clinical practice. Overall, the geometric changes in the tricuspid valve apparatus found in our models reflect clinical findings, and as experimental tool these models permit evaluation of annular geometry and dynamics in FTR with and without associated left-sided dysfunction. Clinical extrapolation requires restraint, as sheep and human TA may differ in anatomy and dynamics, but our previous sonomicrometry experiments in isolated normal beating human hearts[16] have shown similar annular dynamics and geometry to that seen in sheep in vivo.[21] An additional limitation of our study lies in the design, which did not permit acquisition of baseline sonomicrometry data in all groups or examine surgical treatment options.

Conflict of Interest Statement

The authors reported no conflicts of interest.

The *Journal* policy requires editors and reviewers to disclose conflicts of interest and to decline handling or reviewing manuscripts for which they may have a conflict of interest. The editors and reviewers of this article have no conflicts of interest.

References

1. Dreyfus GD, Martin RP, Chan KM, Dulguerov F, Alexandrescu C. Functional tricuspid regurgitation: a need to revise our understanding. *J Am Coll Cardiol*. 2015;65:2331-6. https://doi.org/10.1016/j.jacc.2015.04.011
2. Acar C, Perier P, Fontaliran F, Deloche A, Carpentier A. Anatomical study of the tricuspid valve and its variations. *Surg Radiol Anat*. 1990;12:229-30. https://doi.org/10.1007/BF01624529
3. Calafiore AM, Foschi M, Kheirallah H, Alsaied MM, Alfonso JJ, Tancredi F, et al. Early failure of tricuspid annuloplasty. Should we repair the tricuspid valve at an earlier stage? The role of right ventricle and tricuspid apparatus. *J Card Surg*. 2019;34:404-11. https://doi.org/10.1111/jocs.14042
4. Navia JL, Nowicki ER, Blackstone EH, Brozzi NA, Nento DE, Atik FA, et al. Surgical management of secondary tricuspid valve regurgitation: annulus, commissure, or leaflet procedure? *J Thorac Cardiovasc Surg*. 2010;139:1473-82.e5. https://doi.org/10.1016/j.jtcvs.2010.02.046
5. Teng P, Dai X, Yuan S, Chen Y, Ma L, Ni Y. Tricuspid annulus dilation in patients with combined functional tricuspid regurgitation and left-heart valvular disease: does the septal annulus not dilate? *Front Cardiovasc Med*. 2022;9:1-10.
6. Mathur M, Malinowski M, Timek TA, Rausch MK. Tricuspid annuloplasty rings: a quantitative comparison of size, nonplanar shape, and stiffness. *Ann Thorac Surg*. 2020;110:1605-14. https://doi.org/10.1016/j.athoracsur.2020.02.064
7. Malinowski M, Proudfoot AG, Langholz D, Eberhart L, Brown M, Schubert H, et al. Large animal model of functional tricuspid regurgitation in pacing induced end-stage heart failure. *Interact Cardiovasc Thorac Surg*. 2017;24:905-10. https://doi.org/10.1093/icvts/ivx012
8. Jazwiec T, Malinowski M, Ferguson H, Wodarek J, Quay N, Bush J, et al. Effect of variable annular reduction on functional tricuspid regurgitation and right ventricular dynamics in an ovine model of tachycardia-induced cardiomyopathy. *J Thorac Cardiovasc Surg*. 2021;161:e277-86. https://doi.org/10.1016/j.jtcvs.2019.10.194
9. Verbelen T, Burkhoff D, Kasama K, Delcroix M, Rega F, Meyns B. Systolic and diastolic unloading by mechanical support of the acute vs the chronic pressure overloaded right ventricle. *J Heart Lung Transplant*. 2017;36:457-65. https://doi.org/10.1016/j.healun.2016.10.003
10. Malinowski M, Wilton P, Khaghani A, Langholz D, Hooker V, Eberhart L, et al. The effect of pulmonary hypertension on ovine tricuspid annular dynamics. *Eur J Cardio Thorac Surg*. 2016;49:40-5. https://doi.org/10.1093/ejcts/ezv052
11. Nguyen-Truong M, Liu W, Boon J, Nelson B, Easley J, Monnet E, et al. Establishment of adult right ventricle failure in ovine using a graded, animal-specific pulmonary artery constriction model. *Animal Model Exp Med*. 2020;3:182-92. https://doi.org/10.1002/ame2.12124
12. Prihadi EA, Delgado V, Leon MB, Enriquez-Sarano M, Topilsky Y, Bax JJ. Morphologic types of tricuspid regurgitation: characteristics and prognostic implications. *JACC Cardiovasc Imaging*. 2019;12:491-9. https://doi.org/10.1016/j.jcmg.2018.09.027
13. Addetia K, Muraru D, Veronesi F, Jenei C, Cavalli G, Besser SA, et al. 3-Dimensional echocardiographic analysis of the tricuspid annulus provides new insights into tricuspid valve geometry and dynamics. *JACC Cardiovasc Imaging*. 2019;12:401-12. https://doi.org/10.1016/j.jcmg.2017.08.022
14. Fawzy H, Fukamachi K, Mazer CD, Harrington A, Latter D, Bonneau D, et al. Complete mapping of the tricuspid valve apparatus using three-dimensional sonomicrometry. *J Thorac Cardiovasc Surg*. 2011;141:1037-43. https://doi.org/10.1016/j.jtcvs.2010.05.039
15. Jouan J, Pagel MR, Hiro ME, Lim KH, Lansac E, Duran CM. Further information from a sonometric study of the normal tricuspid valve annulus in sheep: geometric changes during the cardiac cycle. *J Heart Valve Dis*. 2007;16:511-8.
16. Malinowski M, Jazwiec T, Goehler M, Quay N, Bush J, Jovinge S, et al. Sonomicrometry-derived 3-dimensional geometry of the human tricuspid annulus. *J Thorac Cardiovasc Surg*. 2019;157:1452-61.e1. https://doi.org/10.1016/j.jtcvs.2018.08.110
17. Ring L, Rana BS, Kydd A, Boyd J, Parker K, Rusk RA. Dynamics of the tricuspid valve annulus in normal and dilated right hearts: a three-dimensional transoesophageal echocardiography study. *Eur Heart J Cardiovasc Imaging*. 2012;13:756-62. https://doi.org/10.1093/ehjci/jes040
18. Tei C, Pilgrim JP, Shah PM, Ormiston JA, Wong M. The tricuspid valve annulus: study of size and motion in normal subjects and in patients with tricuspid regurgitation. *Circulation*. 1982;66:665-71. https://doi.org/10.1161/01.cir.66.3.665
19. Fukuda S, Saracino G, Matsumura Y, Daimon M, Tran H, Greenberg NL, et al. Three-dimensional geometry of the tricuspid annulus in healthy subjects and in patients with functional tricuspid regurgitation: a real-time, 3-dimensional

echocardiographic study. *Circulation*. 2006;114:I492-8. https://doi.org/10.1161/CIRCULATIONAHA.105.000257
20. Sakon Y, Murakami T, Fujii H, Takahashi Y, Morisaki A, Yamane K, et al. New insight into tricuspid valve anatomy from 100 hearts to reappraise annuloplasty methodology. *Gen Thorac Cardiovasc Surg*. 2019;67:758-64. https://doi.org/10.1007/s11748-019-01092-9
21. Kawada N, Naganuma H, Muramatsu K, Ishibashi-Ueda H, Bando K, Hashimoto K. Redefinition of tricuspid valve structures for successful ring annuloplasty. *J Thorac Cardiovasc Surg*. 2018;155:1511-9.e1. https://doi.org/10.1016/j.jtcvs.2017.12.045
22. Malinowski M, Wilton P, Khaghani A, Brown M, Langholz D, Hooker V, et al. The effect of acute mechanical left ventricular unloading on ovine tricuspid annular size and geometry. *Interact Cardiovasc Thorac Surg*. 2016;23:391-6. https://doi.org/10.1093/icvts/ivw138
23. Kabasawa M, Kohno H, Ishizaka T, Ishida K, Funabashi N, Kataoka A, et al. Assessment of functional tricuspid regurgitation using 320-detector-row multislice computed tomography: risk factor analysis for recurrent regurgitation after tricuspid annuloplasty. *J Thorac Cardiovasc Surg*. 2014;147:312-20. https://doi.org/10.1016/j.jtcvs.2012.11.017
24. Gammie JS, Chu MWA, Falk V, Overbey JR, Moskowitz AJ, Gillinov M, et al. Concomitant tricuspid repair in patients with degenerative mitral regurgitation. *N Engl J Med*. 2022;386:327-39. https://doi.org/10.1056/NEJMoa2115961
25. Rodríguez-Palomares JF, Lozano-Torres J, Dentamaro I, Valente FX, Avilés AS, García-Moreno LG, et al. Predictors of cardiovascular outcomes after surgery in severe tricuspid regurgitation: clinical, imaging and hemodynamic prospective study. *Rev Esp Cardiol*. 2021;74:655-63. https://doi.org/10.1016/j.rec.2020.09.008
26. Isomura T, Hirota M, Hoshino J, Fukada Y, Kondo T, Takahashi Y. Tricuspid annuloplasty with the MC3 ring and septal plication technique. *Asian Cardiovasc Thorac Ann*. 2015;23:5-10. https://doi.org/10.1177/0218492314529953
27. Xu H, Davies H, Zheng J, Peng T, Ni Y. Modified band annuloplasty technique for functional tricuspid regurgitation repair in patients with grossly dilated annuli: the three-suture junctional continuous suture band annuloplasty technique. *J Card Surg*. 2019;34:167-9. https://doi.org/10.1111/jocs.14006
28. Kondoh H, Hatsuoka S, Shintani H. New ring annuloplasty for extremely dilated tricuspid valve annulus: plication to physiologic septal segment size and over-reduction of posterior segment. *Tex Heart Inst J*. 2009;36:327-30.
29. Jazwiec T, Malinowski M, Proudfoot AG, Eberhart L, Langholz D, Schubert H, et al. Tricuspid valvular dynamics and 3-dimensional geometry in awake and anesthetized sheep. *J Thorac Cardiovasc Surg*. 2018;156:1503-11. https://doi.org/10.1016/j.jtcvs.2018.04.065
30. Offen SM, Baker D, Puranik R, Celermajer DS. Right ventricular volume and its relationship to functional tricuspid regurgitation. *Int J Cardiol Heart Vasc*. 2021;38:100940. https://doi.org/10.1016/j.ijcha.2021.100940

Key Words: tricuspid valve, functional tricuspid regurgitation, valve repair

BS

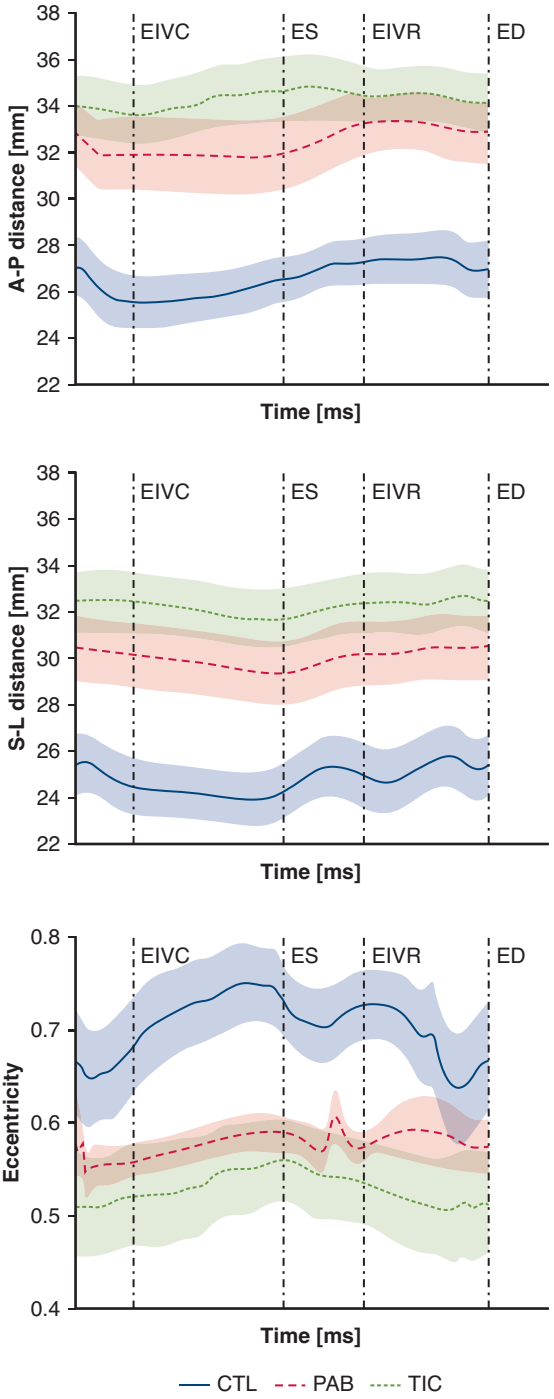

FIGURE E1. Group mean and standard deviation data for anterior–posterior (*top panel*) and septal–lateral (*middle panel*) annular diameters and annular eccentricity (*bottom panel*) throughout the cardiac cycle for CTL (*black line*), PAB (*dashed blue line*), and TIC (*dashed orange line*) animals. *EIVC*, End-isovolumic contraction; *ES*, end-systole; *EIVR*, end-isovolumic contraction; *ED*, end-diastole; *AP*, anterior-posterior commissure; *CTL*, control; *PAB*, pulmonary artery banding; *TIC*, tachycardia-induced cardiomyopathy.

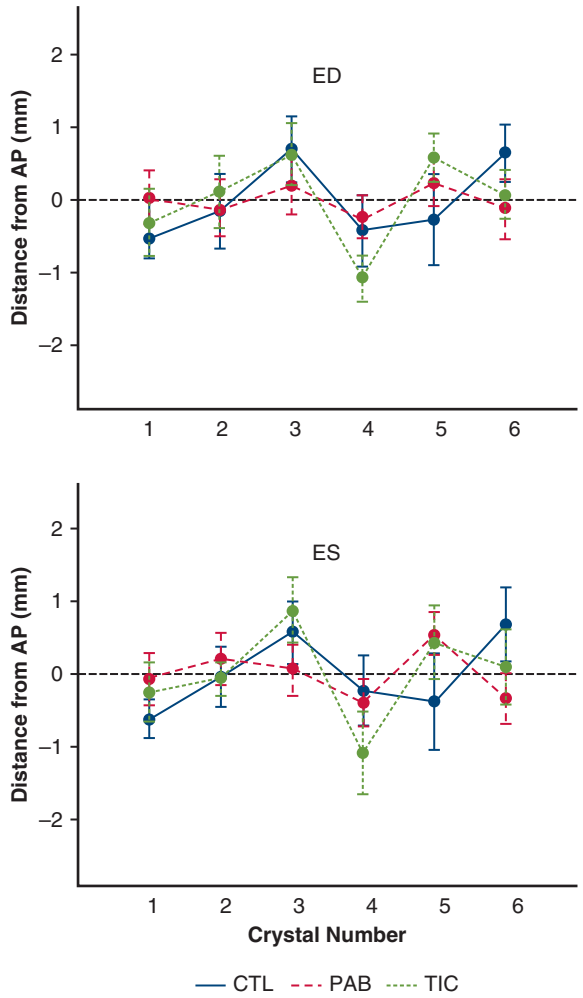

FIGURE E2. Group mean and standard deviation for position of each annular crystal from the least squares annular plane (*dashed line*) at end-diastole (*top panel*) and end-systole (*bottom panel*) for CTL (*black line*), PAB (*dashed blue line*), and TIC (*dashed orange line*) animals. *ED*, End-diastole; *AP*, anterior-posterior commissure; *CTL*, Control; *PAB*, pulmonary artery banding; *TIC*, tachycardia-induced cardiomyopathy; *ES*, end-systole.

BS